Research Square

Preprints are preliminary reports that have not undergone peer review.
They should not be considered conclusive, used to inform clinical practice,
or referenced by the media as validated information.

Fecal Microbiota Transplantation Alleviates Asthmatic Airway Inflammation via the Microbiota–Gut–Lung Axis and Tlrs-IL-33 Signaling

Yilin Zhang
Nanjing Medical University
Liang Ma
The First People's Hospital of Changzhou
Dinghui Qiu
Nanjing Medical University
Zeren Jiang
Nanjing Medical University
Zhiying Huang
Changzhou No.2 People's Hospital
Fei Wang
Changzhou No.2 People's Hospital
Wenwei Luo
Changzhou No.2 People's Hospital
Shuaili Xu
Changzhou No.2 People's Hospital
Liwen Zhang
Changzhou No.2 People's Hospital
Yu Wan
wanyuerke@163.com

Changzhou No.2 People's Hospital

Article

Keywords: Asthma, Fecal microbiota transplantation, Gut–lung axis, Toll-like receptors, IL-33, α-Linolenic acid

Posted Date: June 28th, 2026

DOI: https://doi.org/10.21203/rs.3.rs-10033947/v1

License: This work is licensed under a Creative Commons Attribution 4.0 International License.
Read Full License

Additional Declarations: No competing interests reported.

Abstract

Bronchial asthma is a chronic inflammatory airway disease characterized by type 2 immune dysregulation. Although its pathogenesis remains unclear, current treatments are largely directed at symptoms. Emerging evidence implicates interleukin(IL)-33-driven Th2-type immune responses in asthma development, and disturbances in the gut microbiota (GM) have been suggested to influence pulmonary inflammation via the “gut–lung” axis. We previously reported that children with asthma exhibited high IL-33/sST2 expression, Th1/Th2 imbalance, and significant GM dysbiosis. This study aimed to investigate the role and mechanism of fecal microbiota transplantation (FMT) in modulating airway inflammation in asthma through the TLRs-IL-33 signaling pathway, with the goal of providing a theoretical foundation for microecological interventions in asthma.

Introduction

Bronchial asthma is a chronic inflammatory disorder of the airways characterized by variable airflow limitation, bronchial hyperresponsiveness, and persistent inflammation [1]. Despite the availability of anti-inflammatory and biologic therapies, a substantial proportion of patients remain inadequately controlled [2]. Immunologically, asthma is predominantly driven by type 2 (Th2) inflammation, wherein cytokines as interleukin (IL)-4, IL-5, and IL-13 lead to eosinophilic inflammation, excessive mucus production, and airway remodeling [3].

IL-33, a member of the IL-1 cytokine family, plays a crucial role as an epidermal “alarm hormone” in asthma pathogenesis. It is constitutively expressed in airway epithelial cells and is rapidly released following epithelial injury or environmental stimuli [4]. Engagement of its cognate receptor ST2 potently activates Th2 cells and amplifies type 2 inflammatory responses [5]. Furthermore, elevated serum IL-33 levels, bronchoalveolar lavage fluid (BALF), and airway tissues have been reported and closely correlate with disease severity in patients with asthma [6,7].

Emerging evidence underscores the gut microbiota (GM) as a critical regulator of both systemic and pulmonary immune homeostasis. The concept of the “gut–lung axis” posits that alterations in GM composition and metabolite production influence lung immunity through shared mucosal immune networks and circulating mediators [8]. Consistent with the “hygiene hypothesis,” early-life GM dysbiosis have been linked to a heightened risk of asthma, with antibiotic exposure identified as a risk factor for dis-ease onset and exacerbation [9–11]. Mechanistically, GM-derived signals can regulate dendritic cell function, mediate T cell differentiation, and influence cytokine production, thereby affecting Th1/Th2 balance and immune tolerance [12,13].

Fecal microbiota transplantation (FMT) has recently gained significant attention as an effective method for restoring intestinal microorganism balance [14]. While its therapeutic benefit in gastrointestinal diseases is well-established, research indicates that FMT may also have immunomodulatory effects beyond the gut, including attenuation of allergic airway inflammation [15]. We previously reported marked GM dysbiosis in children with asthma [16]. Interestingly, FMT is linked to reduced IL-33

expression in airway epithelial cells, suggesting a potential mechanistic link between GM regulation and IL-33-driven airway inflammation [12,13].

Toll-like receptors (TLRs) serve as principal pattern-recognition molecules that transduce microbial signals into host immune responses. Components and metabolites from the GM can activate TLRs in immune and epithelial cells, initiating downstream signaling via the MyD88-dependent pathway and regulating cytokine expression, such as IL-33 [17,18]. However, it remains unclear whether GM dysbiosis induces airway inflammation through TLR-dependent IL-33 induction, and whether FMT reverses this process by targeting the TLR–IL-33 axis, remains to be elucidated.

In this study, we aimed to investigate the role and mechanism of FMT in regulating airway inflammation in asthma. We utilized an ovalbumin (OVA)-induced asthma model and MLE-12 cells, and employed molecular, immunological, and metabolomic methods to elucidate how restoring GM homeostasis influences IL-33 secretion, Th1/Th2 immune balance, and airway inflammation. This research may offer new insights into the “gut–lung axis” and provide a theoretical foundation for devel-oping microecosystem-based treatment strategies for bronchial asthma.

Methods

Animal Model

Specific pathogen-free (SPF) BALB/c mice (n = 60; age: 6–8 weeks; weight: 18–20 g) were obtained from the Production Department, Animal Center, Nanjing Medical University. The mice were randomly allocated to six groups (10 mice per group): control group (CTL), sterile group (ABX), model group (OVA), budesonide therapy group (OVA+Bud), FMT therapy group (OVA+FMT), and combined therapy group (OVA+Bud+FMT). All groups except the CTL started consuming sterile water (containing suspensions of 0.5 g/L vancomycin, 1.0 g/L ampicillin, 1.0 g/L neomycin, and 1.0 g/L metronidazole prepared with ultrapure water) at 4 weeks of age to establish sterile models [19]–22]. The ABX group continued to receive sterile water throughout the experiment, whereas the OVA and all therapy groups received sterile water for 2 weeks before switching to ordinary ultrapure water. At the same time, they were sensitized by intraperitoneal injection of 20 μg OVA(Sigma-Aldrich, St. Louis, MO) emulsified in 1 mg aluminum hydroxide (cat.no.PA41005;Nanjing Punoen Biotechnology Co., LTD) (200μL per mouse) for 7 days [23]. Twenty-four hours after the last sensitization, a 5% OVA solution was aerosolized for 40 min daily for 7 days to complete the modeling [24]. Histological staining revealed significant inflammatory cell infiltration in lung tissue, indicating successful model establishment. Starting 24 h after modeling, the OVA+Bud and OVA+Bud+FMT groups received 0.5 mg/mL Bud nebulization therapy for 30 min once daily [25,26]. The OVA+FMT and OVA+Bud+FMT groups received a 0.05 g/mL fecal microbiota enema therapy once daily (100 μL per mouse) [27]–29], with a 2-h interval after aerosolization. After 14 days of therapy, five mice from each group were randomly selected, anesthetized with 50 mg/kg of 1% pentobarbital sodium, and euthanized with an injection of 100 mg/kg pentobarbital sodium. Death was confirmed by respiratory arrest, cardiac arrest, dilated pupils, and absence of neural reflexes. Before

euthanasia, BALF was collected, and blood was drawn from the orbital venous sinuses of anesthetized mice and stored at -80°C. After euthanasia, lung and colon tissues were collected. The remaining mice continued therapy, and after 28 days, samples were collected and euthanized following the same protocol. The detailed procedures are delineated in Fig. 1. The Institutional Animal Care and Use Committee of NMU approved the study protocol (Ref. no. IACUC-2512054).

Cell culture

Mouse alveolar epithelial cells (MLE-12; no. ZQ0470) were obtained from Shanghai Zhongqiao Xinzhou Biotechnology Co., Ltd. and cultured in complete DMEM medium with 2% FBS and 1% P/S (cat. no. ZM0470; Shanghai Zhong Qiao Xin Zhou Biotechnology Co., Ltd.) at 37 °C in a 5% CO_2 incubator. This study aimed to observe the effects of the GM metabolite alpha-linolenic acid (ALA; no. L1499810; Aladdin) on IL-33 secretion by MLE-12 cells. The cells were categorized into three groups: the control group (CTL), the model group (Th2) and the therapy group (Th2+ALA). The therapy group received ALA at 5 μM, 10 μM, and 25 μM. When MLE-12 cells reached 70–80% confluence, they were cultured in serum-free DMEM/F12 for 12 h. The cell suspension was then added to the lower chamber of a Transwell. Stimulation was performed by dissolving cytokine-lyophilized powders (IL-5 at 10 ng/mL, IL-13 at 5 ng/mL, and IL-4 at 1 ng/mL) in pre-cooled sterile PBS and adding them to the culture medium in the lower chamber to contact the MLE-12 cells [30]. After 24 h, the prepared ALA was added to the upper chamber of the Transwell. The cells were returned to the incubator and cultured for an additional 48 h, after which IL-33 concentration levels in each group were measured.

Fecal microbiota suspension

Following the method established by Markus et al. [31], with necessary adjustments, fresh morning fecal specimens were collected from SPF-grade BALB/C mice. The fecal samples underwent quantitative evaluation via culture with a pathogen detection limit of 100 CFU per gram. The feces were dissolved in sterile PBS at a 7:15 (g/mL) ratio, then filtered through stainless-steel sieves with mesh sizes of 2.0, 1.0, 0.5, and 0.25 mm. After centrifuging at 6000 r/min for 15 min, the bacteria were collected, washed three times with sterile PBS, resuspended in 25 mL of PBS solution and stored at 4°C.

ELISA

The mouse ELISA kit was purchased from Shanghai Nuo Yuan Biotechnology Co., LTD, and the provided instructions were followed. Fifty microliters of standard substances at various concentrations were added to standard wells, and 50 μL of the test sample was added to sample wells. Except for blanks, 100 μL of horseradish peroxidase (HRP)-labeled detection antibody was added to both standard and sample wells. The wells were sealed with film and incubated at a constant temperature for 60 min. After plate-washing, 100 μL of mixed chromogenic reagents A and B were added, and the plate was incubated in the

dark at 37°C for 5 min. 50 μL of stop solution were added to each well. The absorbance was measured at 450 nm using a microplate reader to obtain a standard curve and sample concentration. The expression levels of cytokines (IL-2, IL-4, IL-6, IL-10, IL-33, IL-17A, IFN-γ, TNF-α, and sST2) in mouse BALF were measured, and IL-33 and sST2 levels in mouse serum were detected**.**

Reverse transcription quantitative PCR (RT-qPCR)

RT-qPCR was performed by extracting total RNA from 10 mg of lung and colon tissue, as well as from MLE-12 cells (1 x 10^6 cells), using TRIzol® reagent (Invitrogen; Thermo Fisher Scientific, Inc.). cDNA synthesis was performed using HIScript II Q RT SuperMix (Vazyme Biotech Co., Ltd.). Primer sequences are listed in Table 1. The mRNA expression levels were determined by calculating the difference in threshold values between control and experimental genes, using the $2^{-\Delta\Delta cq}$ method, after normalization with GAPDH.

Table 1. Primer sequences used for reverse transcription quantitative PCR.

Gene	Primer sequence (5‘-3‘)
IL-33	F:CAGAAGACCAAGAATTCTGCC
	R:CATGCTTGGTACCCGATTTTAG
TLR2	F:CTCTTCAGCAAACGCTGTTCT
	R:GGCGTCTCCCTCTATTGTATTG
TLR4	F:TTTGACACCCTCCTAGACTTCA
	R:GAAACTGCAATCAAGATGCTG
IRAK	F:GGACTTCCACATTCGAGGTAC
	R:GGTCTTTGCACCTTGTGTCCTC
TRAF6	F:AAAGCGAGAGATTCTTTCCCTG
	R:ACTGGGGACAATTCACTGAGC
MyD88	F:ATCGCTGTTCTTGAACCCTCG
	R:CTCACGGTCTAACAAGGCCAG
ZO-1	F:GCCGCTAAGAGCACAGCAA
	R:GCCCTCCTTTTAACACATCAGA

Western blot

The analysis was conducted using RIPA lysis buffer (R301899; Aladdin), phenylmethylsulfonyl fluoride protease inhibitor (ST2573; Beyotime Institute of Biotechnology), and a phosphatase inhibitor (RFZ-RP-5041; Beyotime Institute of Biotechnology), which were added to lung and intestinal tissues (10 mg, ground with a tissue grinder) and MLE-12 cells (1×10^6) at a 100:1:1 ratio. The mixture was placed on ice for 30 min before being centrifuged at 12,000 rpm at 4°C for 5 min. The supernatant was then transferred to a new EP tube. The protein concentration was determined using a BCA protein quantification kit (Shanghai Biyun Tian Biotechnology Co., Ltd.). Proteins were separated by 8% sodium dodecyl sulfate-polyacrylamide gel electrophoresis and transferred onto PVDF membranes (BS-PVDF-45-S; Biosharp). After blocking, the membranes were incubated overnight at 4°C with primary antibodies (all at 1:1000): GAPDH (PB1034; Nanjing Punoen Biotechnology Co., Ltd), IL-33 (66235-1-Ig; Wuhan Sanying Biotechnology Co., Ltd), TLR2 (BD-PB1447; Suzhou Botlong Immune Technology Co., Ltd), TLR4 (19811-1-AP; Nanjing Punoen Biotechnology Co., Ltd), MyD88 (RM8802; Suzhou Botlong Immune Technology Co., Ltd), IRAK (BD-PT2391; Suzhou Botlong Immune Technology Co., Ltd), TRIF (RM9023; Suzhou Botlong Immune Technology Co., Ltd), P65 (RM8927; Suzhou Botlong Immune Technology Co., Ltd), p-P65 (RM8589; Suzhou Botlong Immune Technology Co., Ltd), IKBa (RM8349; Suzhou Botlong Immune Technology Co., Ltd) and p-IKBa (RM8843; Suzhou Botlong Immune Technology Co., Ltd). The PVDF membrane was incubated with secondary antibodies at room temperature for 1 h. The secondary antibody used (1:2000) was an HRP-bound rabbit anti-mouse antibody (PWH054; Nanjing Punoen Biotechnology Co., Ltd). Protein bands were visualized using chemiluminescent reagents, and ImageJ software 1.8.0 (National Institutes of Health) was used for semi-quantitative normalization to GAPDH or P65.

Hematoxylin and eosin (HE) staining

Initially, fresh lung and intestinal tissues were fixed in 4% formaldehyde at room temperature for 24 h and then soaked overnight in 75% ethanol. After dehydration through ethanol gradients, the tissues were placed in xylene I, II, and III for 1 h each to achieve transparency and then immersed in paraffin overnight. Sections (3-μm thick) were cut using a paraffin sectioning machine and attached to slides for structural integrity observation. For dewaxing, sections were placed in xylene I, II, and III for 10 min each, dehydrated in an ethanol gradient, and rinsed with running water for 5 min. Hematoxylin staining was performed for 10 min, and the sections were soaked in ultrapure water for 15 min. Then, eosin staining was applied for 5 min, and the reaction was terminated by a 15-s immersion in ultrapure water. Gradient dehydration and transparency treatments were repeated. Finally, the section was sealed with neutral gum and inflammatory cell infiltration in mouse lung tissue was observed using a high-resolution panoramic imaging system.

Immunohistochemical (IHC) analysis

IHC analysis was conducted on frozen tissues sectioned into 5 μm ultrathin slices. The sections were fixed with cold acetone, rinsed with PBS, and incubated with 3% hydrogen peroxide. After treatment with microwave citric acid buffer and heating-cooling, primary antibodies (TLR2, TLR4, and ZO-1) were added and incubated overnight at 4°C. The secondary antibody (HRP combined with goat anti-mouse antibody) was then added and incubated at room temperature for 20 min. Next, the sections were rinsed with DAB for color development and stained with hematoxylin for 30 s. Differentiation was performed using hydrochloric acid and alcohol, followed by thorough rinsing with distilled water. After counterstaining, the sections were dehydrated using an alcohol gradient. Finally, they were made transparent and sealed with a neutral gel. The number of positive cells was counted, and the percentage of cells with positive nuclei relative to the total number of cells was calculated.

Cell Counting Kit-8 (CCK-8)

Equal numbers of MLE-12 cells were seeded into a 96-well plate and incubated in DMEM with 2% FBS and 1% P/S at 37°C with 5% CO_2 for 24 h. ALA at concentrations of 0, 5, 10, 25, 50 and 100 μM was then added to the plate [32], and the cells were further incubated at 37°C with 5% CO_2 for either 24 or 48 h. Afterward, 10 μL of CCK-8 solution was added to each well, and the plate was incubated again at 37 °C with 5% CO_2 for 1–4 h. The absorbance at 450 nm was measured.

16S rRNA sequencing

On days 14 and 28, fecal samples from mice in the CTL, ABX, OVA and therapy groups were collected and immediately frozen at -80°C. This procedure ensures the stability of the microbial community structure, preventing alterations due to environmental changes. Genomic DNA was extracted from the fecal samples to obtain high-purity DNA. Using the extracted DNA as a template, PCR amplification was performed with synthesized primers. The resulting PCR products were purified and used to construct a sequencing library. Libraries that passed quality inspection were sequenced on the Illumina HiSeq platform for high-throughput analysis. Trimmomatic (v0.36) and Pear (v0.9.6) software were employed for raw data quality control, whereas QIIME (v.1.8.0) and R software facilitated data analysis. This experiment was supported and conducted by Shanghai GeneCowin Biotechnology Co., Ltd.

Metabolomics analysis

The analysis involved examining the distribution of positive and negative ion metabolites across various KEGG pathways in the CTL, ABX, OVA, and therapy groups.

Statistical analysis

All data were statistically analyzed and plotted using GraphPad Prism 10, SPSS 25.9, and R 4.5.1 software. Comparisons between two groups of data were performed using paired t-tests, while differences among multiple groups were evaluated using one-way analysis of variance (ANOVA), repeated measures ANOVA (data show means + SD), or the Kruskal–Wallis test (data are presented as medians and interquartile ranges). Statistical significance was set at P-values <0.05.

Results

FMT alleviates airway inflammation in asthmatic mice

Lung tissue sections were examined by HE staining to assess peribronchial and perivascular inflammatory infiltration. Histological scoring was performed according to the criteria established by Ren et al. [33] (Fig. 2a). As shown in this figure, in the OVA stimulation group, mice had significant inflammatory cell accumulation around the bronchi and blood vessels, airway wall thickening, and structural disorders. By day 14, all therapy groups showed alleviated airway inflammatory cell infiltration; this effect was most pronounced in the OVA + Bud+FMT group. By day 28, pulmonary inflammation was further ameliorated, and the D-28 OVA + Bud+FMT nearly restored normal lung structure, similar to that in the CTL group. Lung tissue pathological grading scores confirmed these findings, as scores decreased in the Bud/FMT alone therapy group and were even lower in the combined therapy group. These findings suggest that FMT partially alleviates OVA-induced pulmonary inflammation and exerts a synergistic effect when combined with budesonide.

FMT modulates immune imbalance in allergic airway inflammation

To investigate the immunomodulatory effect of FMT, we measured Th1 Th2 and Th17 type cytokines in each group of mice on the 14th and 28th days after OVA induction (Fig. 2b-d). Results showed OVA significantly suppressed Th1-type cytokine expression and increased Th2/Th17-type cytokine levels. Compared to the OVA group, both the Bud and FMT groups showed partially restored Th1-type cytokine expression and reduced Th2/Th17-type cytokine levels, showing immunomodulatory effects. On day 14, neither Bud nor FMT alone reduced Th17-type cytokine levels, possibly due to hormone resistance and inflammatory redistribution [34–37]. However, the OVA + Bud+FMT group showed a significant decrease. By day 28, IL-17A levels decreased significantly in all therapy groups. Temporal dynamic analysis revealed that over time (Fig. 2e), Th1-type cytokines in each intervention group increased, whereas Th2- and Th17-type cytokines decreased, with the OVA + Bud+FMT group having the most pronounced changes. In conclusion, FMT effectively corrected OVA-induced Th1/Th2/Th17 imbalance and synergizes with budesonide to accelerate the restoration of immune homeostasis.FMT decreases IL-33/sST2 levels in serum and BALF.

FMT decreases IL-33/sST2 levels in serum and BALF

To determine whether FMT modulates the epithelial alarmin axis, we measured IL-33 and its soluble receptor sST2 in serum and BALF (Fig. 3a, b). The findings showed that OVA significantly increased IL-33/sST2 levels in both serum and BALF compared with those in the CTL group, indicating activation of the IL-33-related signaling pathway. Either Bud or FMT alone reduced IL-33/sST2 levels to some extent, whereas combined Bud and FMT therapy had a more obvious effect. Temporal dynamic analysis from days 14 to 28 (Fig. 3c) revealed that the therapy groups, especially the combined Bud and FMT group, significantly accelerated the decline in sST2 levels. These data demonstrate that FMT effectively attenuates OVA-induced IL-33/sST2 axis activation, thereby dampening upstream pro-inflammatory signals that drive type 2 immunity.

FMT inhibits TLR2/4–MyD88–NF-κB signaling in lung tissue

To investigate whether FMT interferes with TLR-mediated innate immune signaling, we examined TLR2, TLR4, and their key downstream signaling molecules in mouse lung tissues. IHC results (Fig. 3d) showed increased TLR expression in the OVA group, whereas TLR2/4 receptor expression decreased in all three therapy groups. Treatment effectiveness was ranked as follows: OVA + Bud+FMT > OVA+Bud > OVA+FMT, with better outcomes on day 28 than on day 14. Western blot analysis indicated that the OVA group significantly upregulated TLR2, TLR4, MyD88, IRAK, TRAF6 and p-P65 expressions (Fig. 3e and Supplementary Fig. S1), suggesting continuous activation of the TLRs–MyD88–NF-κB signaling pathway. Bud or FMT reduced the expression of TLR2/4 and its downstream molecules, and the OVA + Bud+FMT exhibited the most substantial inhibitory effect at each time point, normalizing their expression. The qRT-PCR results were consistent with changes in protein level (Fig. 3f). Collectively, these results indicate that FMT potently suppresses aberrant activation of the TLR2/4–MyD88–IRAK–TRAF6–NF-κB signaling axis, suggesting that blockade of TLR-mediated signal transduction contributes to its anti-inflammatory effect in allergic airway.

FMT ameliorates OVA-induced colonic injury

To evaluate the effect of FMT on intestinal pathology, we analyzed body weight changes and the disease activity index (DAI) [38] (Fig. 4a, with DAI scoring criteria in Table 2), and examined colonic tissue's histological morphology and inflammation score (Fig. 4b). Compared with the CTL group, OVA-group mice had significant weight loss and a marked increase in DAI score, indicating a worsened systemic condition and intestinal inflammation. After the intervention, Bud partially mitigated weight loss and decreased the DAI score. FMT intervention significantly improved weight trends and lowered DAI scores throughout the observation period. OVA + Bud+FMT had the most pronounced effects on weight recovery and DAI reduction. HE staining revealed severe colonic mucosal damage in the OVA group. Both Bud and FMT alleviated inflammatory responses and structural damage. The FMT group showed intact mucosal structures and greater improvement in inflammatory infiltration. The OVA + Bud+FMT group showed the most substantial recovery of intestinal structure and inflammatory infiltration. The histological scores were consistent with HE-staining observations. These results suggest that FMT

effectively alleviates colonic tissue damage by preserving intestinal structure and inhibiting inflammation.

Table 2
Disease activity index scoring system of dextran sodium sulfate-induced colitis.

Score	Weight loss (%)	Stool consistency	Blood in feces
0	No weight loss	Normal	Normal
1	1–5	Loose stool	Positive fecal occult blood
2	> 5–10		
3	> 10–15		
4	> 15	Pasty or thin water stool	Visible blood in feces

FMT enhances the transcription and expression of tight junction proteins in intestinal epithelial cells

To determine whether FMT promotes repair of the intestinal epithelial barrier, we assessed the localization, protein expression, and transcriptional regulation of the tight junction protein ZO-1 in colon tissue. IHC analysis (Fig. 4c) showed that, in the CTL group, ZO-1 was consistently distributed along colonic epithelial cell membranes. In contrast, the OVA group showed significantly weakened and discontinuous ZO-1 staining, indicating intestinal epithelial tight junction damage. Both Bud and FMT interventions increased ZO-1 staining intensity and continuity in the colonic epithelium, with greater recovery observed in the FMT group than the Bud group. The combined therapy restored ZO-1 distribution to CTL-group levels at both time points. Western blot analysis (Fig. 4d) confirmed these findings, as the OVA group showed decreased ZO-1 protein expression, which was reversed by Bud and FMT. The qRT-PCR results (Fig. 4e) showed that OVA + Bud+FMT further enhanced ZO-1 mRNA expression, suggesting a synergistic transcriptional effect. Collectively, these findings indicate that FMT effectively enhances ZO-1 transcription and expression at both mRNA and protein levels, facilitates its proper membrane localization, and thereby contributes to the restoration of intestinal epithelial barrier function.

FMT reshores GM diversity and composition

To systematically assess evaluate the effect of FMT on GM structure, we per-formed 16S rRNA sequencing analysis of fecal samples from each group of mice. We compared α-diversity, β-diversity, community composition, and changes in key differential microbiota. The α-diversity analysis indicated that by day 14, OVA treatment significantly diminished GM richness and diversity (Fig. 5a). This was evidenced by decreases in the observed species and Chao1, ACE, and Shannon indices, whereas the Simpson's index increased, indicating impaired diversity. In contrast, the OVA + Bud+FMT significantly enhanced these diversity indices, with some metrics approaching control group levels. By day 28, no

significant differences were observed in the Shannon and Simpson indices among the groups, indicating a gradual convergence of the microbial community structure.

β-diversity analysis using principal coordinate analysis revealed distinct separation of GM profiles among the groups at two time points (Fig. 5b), indicating that the therapy methods influenced the overall microbiota structure. The OVA and CTL groups showed significant spatial separation. Notably, after FMT therapy, the samples began to cluster closer to the CTL. Samples treated with both Bud and FMT clustered most closely with CTL, suggesting that FMT effectively reshaped the OVA-induced abnormal intestinal flora structure.

The Venn diagram analysis (Supplementary Fig. S2a) revealed that on day 14, only 86 core average operational taxonomic units (OTUs) were shared across all groups, and each group had a substantial number of specific OTUs. However, by day 28, the shared core OTUs among the six groups significantly increased to 215. FMT therapy significantly increased the number of OTUs shared with the CTL group, helping to restore health-related microbiota characteristics. As the intervention period extended, the OTU composition in each group converged, forming a larger common core microbiota.

On day 14, at the phylum level (Fig. 5c), the CTL group's intestinal flora was mainly composed of Bacillota and Bacteroidota, with a stable structure. In the OVA group, the microbiota composition was disrupted, with an imbalanced Bacillota-to-Bacteroidota ratio and an increased in abnormal phyla such as Pseudomonadota. The OVA + Bud group showed slightly improved microbiota structure but did not fully restore it. FMT intervention significantly increased the abundance of Bacillota and Bacteroidota, making the microbiota structure closer to that of the CTL group. The OVA + Bud+FMT group showed the most significant recovery. By day 28, its microbiota structure was similar to that of the CTL group. At the genus level (Supplementary Fig. S2b), on day 14, the CTL group contained mainly symbiotic bacteria related to Muribaculaceae, Bacteroides, Lactobacillus, and Blautia. In contrast, in the OVA group, genera related to Bacteroides and Muribaculaceae decreased significantly. Bud therapy partly reduced these abnormally elevated bacterial genera; however, the overall recovery was limited. FMT intervention significantly increased the abundance of genera such as Bacteroides, Prevotella, Lachnospiraceae_NK4A136_group, and Ruminococcus, and the OVA + Bud+FMT group showed the most complete recovery. By day 28, the bacterial genus composition of the therapy groups was similar to that of the CTL group.

To elucidate the impact of various treatments on the differential characteristics of intestinal flora, we employed LEfSe analysis with linear discriminant analysis (LDA) (Fig. 5d) to identify the distinct flora in each group at different time points. By day 14, the CTL group was significantly enriched in Blautia, Lachnospiraceae bacterium, Tannerellaceae, Parabacteroides, and their related phylogenetic branches. In contrast, the OVA group showednotable enrichment of Erysipelatoclostridium and Clostridia-related genera. The OVA + Bud group was mainly enriched in Lactobacillaceae, Lactobacillus, and Ligilactobacillus. The OVA + FMT group showed significantly higher levels of Bifidobacteriaceae and Bifidobacterium. The OVA + Bud+FMT group was enriched with multiple symbiotic genera, including

Muribaculaceae, Lachnospiraceae_NK4A136_group, and Ruminococcaceae, with the microbiota structure significantly returning to normal according to the LDA scores and phylogenetic distribution. By day 28, the OVA + Bud group showed enrichment in Butyricicoccus, Anaerotruncus, and Romboutsia. The OVA + FMT group was enriched with symbiotic genera, such as Candidatus_Saccharimonas and Eubacterium_ventriosum_group. The OVA + Bud+FMT group had the most significant microbiota remodeling effect, with enrichment across multiple branches of health-related phylogenetic systems, and its LDA score distribu-tion closely resembled that of the CTL group.

These results demonstrate that FMT effectively addresses the GM imbalance caused by OVA, restores microbiota diversity, and reshapes the overall microecological structure, providing a microbial basis for its protective effects on the gut–lung axis.

FMT induces broad metabolic reprogramming

To explore the functional consequences of GM remodeling, we performed pathway enrichment analysis on the differential metabolites (Supplementary Fig. S2c). On day 14, metabolic pathway enrichment analysis revealed significant enrichment in energy and amino acid metabolism pathways. By day 28, the pathway enrichment pattern had further evolved. The TCA cycle, cofactor biosynthesis, glucose metabolism, energy homeostasis pathways (glycolysis/gluconeogenesis and pentose phosphate pathways), and various amino acid metabolic pathways continued to show significant enrichment. Notably, the intestinal IgA pathway emerged only on day 28, suggesting a shift from metabolic to immune regulation in the gut–lung axis. These data indicate that FMT triggers profound metabolic remodeling affecting both energy supply and immune homeostasis, supporting the concept of a “microecological–metabolic–immune” axis.

Identification of α-linolenic acid (ALA) as a key FMT-responsive metabolite

To identify potential metabolic mediators of FMT’s anti-inflammatory effect, we performed non-targeted metabolomic analyses on the samples to systematically assess differential metabolite profiles and their correlation characteristics (Fig. 5e and Supplementary Fig. S2d). Differential metabolite clustering analysis showed that on days 14 and 28, metabolite expression patterns were clearly separated between groups. After FMT treatment, the samples’ overall metabolic profile gradually resembled that of the control group, indicating that FMT could reverse the OVA-induced abnormal metabolic state. Heat map analysis showed significant remodeling of lipid-related metabolites in the FMT group, especially unsaturated fatty acid-related ones. Correlation analysis of two nodes revealed a coordinated relationship among differentially expressed metabolites. ALA and its downstream metabolites showed significant differences at both time points and were strongly correlated with multiple metabolites, suggesting that they may be key components of the metabolic regulatory network. ALA abundance in the OVA + FMT group was higher than in the OVA group, indicating a link with the GM state. Given ALA’s role in modulating inflammation and immune homeostasis, we hypothesized that ALA could be a key

metabolic mediator in the FMT-mediated axis. Based on non-targeted metabolomics and correlation analysis, we identified ALA as the key metabolite for further research and confirmed its role in inflammation modulation through cell experiments.

The effect of ALA on MLE-12 cells viability

To establish a safe and effective dosage range for subsequent mechanistic studies, we evaluated the impact of ALA on MLE-12 cell viability using the CCK-8 assay. Cells were exposed to 0, 5, 10, 25, 50, and 100 μM ALA for 24 and 48 h and cell viability was analyzed (Fig. 6a). The results showed that 5 μM and 10 μM ALA for 24 or 48 h had no significant impact on cell viability, with survival rates similar to the control group. At 25 μM, ALA had a mild effect on cell viability after 24 h, and although the survival rate slightly decreased at 48 h, it remained above 85%, indicating no apparent cytotoxicity. In contrast, 50 and 100 μM ALA significantly reduced cell viability at both 24 and 48 h, showing a dose-dependent decline. Considering cell viability, safety and the needs of subsequent experiments, 5, 10, and 25 μM ALA were selected for further cell experiments. A 48-h treatment was used to evaluate ALA's regulatory effect on IL-33 expression and the associated signaling pathways.

ALA suppresses IL-33 secretion in MLE-12 cells in a dose-dependent manner

To determine whether ALA directly regulates IL-33 expression in airway epithelial cells, we treated MLE-12 cells with ALA at the selected non-cytotoxic concentrations under Th2-cytokine stimulation. Cells were assigned to seven groups: Control, Vehicle, Model, Model + ALA-L (5 μM ALA), Model + ALA-M (10 μM ALA), Model + ALA-H (25 μM ALA), and ALA alone (25 μM ALA). Western blot analysis showed that ALA treatment markedly reduced intracellular IL-33 protein levels compared to the Model group, and this inhibition intensified with increasing ALA concentrations (Fig. 6b). Moreover, qRT-PCR analysis revealed that Model stimulation upregulated IL-33 mRNA expression, whereas ALA treatment downregulated IL-33 transcription in a dose-dependent manner (Fig. 6c), consistent with Western blot results. Results from both methods showed that ALA significantly inhibits IL-33 expression in MLE-12 cells induced by model stimulation, affecting transcription and protein expression without evident cytotoxicity. This finding indicate that ALA directly inhibits IL-33 transcription and translation in inflamed airway epithelial cells without detectable cytotoxicity.

ALA inhibits the activation of the TLR2/4-MyD88-IRAK-TRAF6-NF-κB pathway

To investigate whether ALA suppresses IL-33 expression by interfering with TLR-mediated signaling, we treated MLE-12 cells with the TLR4 agonist lipopolysaccharide (LPS) and the TLR2 agonist Pam3CSK4 following model stimulation. We then assessed the transcriptional levels of *TLR2/4* and the activation status of downstream signaling molecules. Cell experiments comprised eight groups: Control, Model, Model + ALA, Model + LPS, Model + ALA + LPS, Model + Pam3CSK4, Model + ALA + Pam3CSK4, and

Model + ALA + Pam3CSK4 + LPS. The qRT-PCR results showed that model stimulation significantly increased TLR2 and TLR4 mRNA expression in MLE-12 cells compared to the control group (Fig. 6d). The addition of LPS or Pam3CSK4 to the model further increased TLR2/4 transcription levels, indicating TLR2/4 signaling pathway activation. ALA intervention markedly inhibited the upregulation of TLR2 and TLR4 expression induced by model stimulation and LPS or Pam3CSK4, even under combined stimulation, suggesting a direct intervention in TLR2/4 activation. Western blotting results (Fig. 6e) confirmed ALA's inhibitory impact on downstream TLR signaling pathways. Model stimulation significantly increased MyD88, p-IκBα, and p-P65 expression, indicating TLR2/4-MyD88-NF-κB pathway activation. LPS or Pam3CSK4 enhanced this activation. ALA treatment reduced MyD88 expression and inhibited p-IκBα and p-P65, blocking TLR2/4 downstream signals to NF-κB. These findings suggest that ALA reduces IL-33 expression triggered by inflammatory stimuli by inhibiting the TLR2/4-MyD88-IRAK-TRAF6-NF-κB signaling pathway, providing direct molecular evidence for its role in modulating the inflammatory response in epithelial cells.

Discussion

In this study, we showed that FMT significantly reduced allergic airway inflammation induced by OVA in a mouse model and clarified the mechanism connecting GM changes to the regulation of epithelial innate immunity. Our findings reveal that FMT modulates immune responses via the "gut–lung" axis, beginning with decreased pulmonary inflammatory infiltration and culminating in the suppression of the TLR2/4-MyD88-IRAK-TRAF6-NF-κB signaling pathway by ALA.

Our findings are consistent with those of earlier studies, indicating that asthma involves systemic immune dysregulation. We demonstrated that FMT significantly reduced inflammatory cell infiltration in lung tissues, suppressed airway inflammation, and rebalanced Th1/Th2/Th17 immune responses in asthmatic mice. Concurrently, FMT markedly decreased the expression of epithelial-derived alarmins, such as IL-33 and sST2, suggesting that targeting epithelial innate immune activation is crucial for FMT-mediated protection. Since IL-33 plays a central role in amplifying type 2 immune responses, its suppression likely explains the reduced airway inflammation observed after FMT.

The protective effects of FMT were not only comparable to but also complemented those of Bud, a primary anti-inflammatory treatment for asthma. In various outcome measures, such as airway inflammatory infiltration, cytokine production, epithelial barrier integrity, and innate immune signaling, the combined Bud and FMT therapy consistently yielded more significant improvements than either intervention alone. This synergistic effect was especially noticeable at the later stages, indicating that FMT may enhance or prolong the anti-inflammatory effectiveness of corticosteroid therapy.

Our data revealed a distinct time-dependent pattern in the therapeutic effects of FMT. Notably, significant improvements were evident by day 14, but the protective effects of FMT, whether used alone or in combination with Bud, were more pronounced by day 28. This temporal enhancement was consistent across lung inflammation, intestinal barrier restoration, GM remodeling, and the suppression of TLR-

mediated signaling pathways. These findings indicate that FMT exerts a progressive and cumulative regulatory effect, likely due to the time required for stable microbial engraftment and metabolic reprogramming.

Furthermore, FMT's protective effects extend beyond the lungs. Our observations revealed that OVA-induced asthma led to significant colonic injury, an elevated disease activity index, and compromised intestinal epithelial integrity, as demonstrated by the decreased expression of the tight junction protein ZO-1. FMT significantly alleviated colonic histopathological damage and restored ZO-1 expression at both the transcriptional and protein levels, suggesting recovery of intestinal barrier function. These findings support the idea that disruption of the intestinal barrier may contribute to systemic inflammatory signaling during allergic airway inflammation and that restoring gut integrity is a crucial upstream event in FMT-mediated immune regulation.

At the molecular level, we showed that FMT suppressed TLR signaling activation in lung tissues. The OVA challenge significantly upregulated TLR2 and TLR4, along with downstream adaptors and signaling molecules, such as MyD88, IRAK, TRAF6, and p-P65. FMT therapy significantly decreased the expression and activation of these signaling components, suggesting that inhibition of TLR-mediated innate immune signaling may be key to FMT's anti-inflammatory effects. Notably, the combination of Bud and FMT therapy resulted in the most substantial suppression of this pathway, indicating a synergistic mechanism between microbial modulation and pharmacological anti-inflammatory intervention.

To investigate how GM changes due to FMT affects immune signaling, we con-ducted extensive GM and metabolomic analyses. FMT reshaped the gut microbial community, restoring both diversity and composition to a healthier state. This microbial transformation is linked to significant metabolic reprogramming, particularly in pathways involving energy, amino acid, and lipid metabolism. Notably, ALA consistently appeared as a crucial metabolite, with its levels reduced in asthmatic mice, but restored after FMT.

Building on these in vivo observations, in vitro experiments showed that ALA directly inhibited IL-33 expression in airway epithelial cells at the transcriptional and protein levels without causing cytotoxicity. Mechanistically, ALA reduced TLR2/4-mediated activation of the MyD88–IRAK–TRAF6–NF-κB signaling pathway, even when stimulated by agonists. These findings suggest that ALA serves as a functional metabolic mediator, connecting FMT-induced microbial changes to the suppression of epithelial innate immune activation.

In conclusion, this study provides comprehensive evidence that FMT alleviates allergic airway inflammation through a mechanism involving GM remodeling, enrichment of ALA, and subsequent suppression of the TLR2/4–MyD88–NF κB–IL-33 signaling axis in airway epithelial cells. The observed synergy with budesonide and the time dependent amplification of therapeutic benefits position FMT as a promising adjunctive strategy for asthma management. Our findings underscore the therapeutic potential of targeting the gut–lung axis and provide a rationale for future clinical trials investigating microbiota based interventions in allergic airway diseases.

Declarations

Acknowledgments

We would like to thank Shanghai GeneCowin Biotechnology Co., Ltd. with processing and analyzing scRNA-seq data and all participants in this study for their dedication and cooperation. We would like to thank Editage (www.editage.jp) for English language editing.

Funding Declaration

This research was funded by grants from the Top Talent of Changzhou “The 14th Five-Year Plan” High-Level Health Talents Training Project (2022260; 2024BJHB013), The National Natural Science Foundation of China (No. 82400025),Technology Bureau Applied Basic Research Program (CJ20245023), and The Jiangsu Princial Health Commissic Medical Research Youth Project (MO2024001); Nursing-Specific Scientific Research Project of Changzhou No.2 People’s Hospital (CDHL202510).

Author Contributions

Y.W. designed the study. Y.Z., L.M. and L.Z. performed the experiments and wrote the manuscript. Y.Z., D.Q. and Z.J. contributed to the data analysis. Z.H., F.W. and W.L. confirm the authenticity of all the raw data. All authors have read and approved the final manuscript.

Data Availability Statement

The datasets generated and/or analysed during the current study are available in the NCBI repository, [PRJNA1479535].

Ethics approval and consent to participate

All animal experiments in this study were conducted in strict accordance with the ethical guidelines and standards set by the Institutional Animal Care and Use Committee of Nanjing Medical University (Ref. no. IACUC-2512054).

Consent for publication

Not applicable.

Competing interests

The author(s) declare no competing interests.

References

1. Celeste, P.; Erik, M.; Lauri, L.; Dominick, S. Lancet (London, England), asthma **2023**, *401*, 858–873. DOI:10.1016/S0140-6736(22)02125-0.
2. Jaclyn, Q.; J.K.H.; Jorge, M.; et al. Allergy, asthma, and clinical immunology: official journal of the Canadian Society of Allergy and Clinical Immunology, Asthma[J] **2018**, *14*(supplement 2), 50. DOI:10.1186/s13223-018-0279-0.
3. Mukherjee, M.; Nair, P. Autoimmune responses in severe asthma. *Allergy Asthma Immunol Res* **2018**, *10*, 428–447. DOI:10.4168/aair.2018.10.5.428.
4. Smith, D.E. IL-33: A tissue derived cytokine pathway involved in allergic inflammation and asthma. *Clin Exp Allergy* **2010**, *40*, 200–208. DOI:10.1111/j.1365-2222.2009.03384.x.
5. Schmitz, J.; Owyang, A.; Oldham, E.; Song, Y.; Murphy, E.; McClanahan, T.K.; Zurawski, G.; Moshrefi, M.; Qin, J.; Li, X.; et al. IL-33, an interleukin-1-like cytokine that signals via the IL-1 receptor-related protein ST2 and induces T helper type 2-associated cytokines. *Immunity* **2005**, *23*, 479–490. DOI:10.1016/j.immuni.2005.09.015.
6. Bahrami Mahneh, S.; Movahedi, M.; Aryan, Z.; Bahar, M.A.; Rezaei, A.; Sadr, M.; Rezaei, N.; Universal Scientific Education and Research Network (USERN). Serum IL-33 is elevated in children with asthma and is associated with disease severity. *Int Arch Allergy Immunol* **2015**, *168*, 193–196. DOI:10.1159/000442413.
7. Guo, Z.; Wu, J.; Zhao, J.; Liu, F.; Chen, Y.; Bi, L.; Liu, S.; Dong, L. IL-33 promotes airway remodeling and is a marker of asthma disease severity. *J Asthma* **2014**, *51*, 863–869. DOI:10.3109/02770903.2014.921196.
8. Hufnagl, K.; Pali-Schöll, I.; Roth-Walter, F.; Jensen-Jarolim, E. Dysbiosis of the gut and lung microbiome has a role in asthma. *Semin Immunopathol* **2020**, *42*, 75–93. DOI:10.1007/s00281-019-00775-y.
9. Arrieta, M.C.; Stiemsma, L.T.; Dimitriu, P.A.; Thorson, L.; Russell, S.; Yurist-Doutsch, S.; Kuzeljevic, B.; Gold, M.J.; Britton, H.M.; Lefebvre, D.L.; et al. Early infancy microbial and metabolic alterations affect risk of childhood asthma. *Sci Transl Med* **2015**, *7*, 307ra152. DOI:10.1126/scitranslmed.aab2271.
10. Ni, J.; Friedman, H.; Boyd, B.C.; McGurn, A.; Babinski, P.; Markossian, T.; Dugas, L.R. Early antibiotic exposure and development of asthma and allergic rhinitis in childhood. *BMC Pediatr* **2019**, *19*, 225. DOI:10.1186/s12887-019-1594-4.
11. Kozik, A.J.; Huang, Y.J. The microbiome in Asthma: Role in pathogenesis, phenotype, and response to treatment. *Ann Allergy Asthma Immunol* **2018**, *122*, 270–275. DOI:10.1016/j.anai.2018.12.005.
12. Maynard, C.L.; Elson, C.O.; Hatton, R.D.; Weaver, C.T. Reciprocal interactions of the intestinal microbiota and immune system. *Nature* **2012**, *489*, 231–241. DOI:10.1038/nature11551.
13. Luda, K.M.; Joeris, T.; Persson, E.K.; Rivollier, A.; Demiri, M.; Sitnik, K.M.; Pool, L.; Holm, J.B.; Melo-Gonzalez, F.; Richter, L.; et al. IRF8 transcription-factor-dependent classical dendritic cells are essential for intestinal T cell homeostasis. *Immunity* **2016**, *44*, 860–874. DOI:10.1016/j.immuni.2016.02.008.

14. Gu, J.L.; Wang, Y.Z.; Liu, S.Y.; Yu, G.J.; Zhang, T.; Lu, H. Gut microbiota community adaption during young children fecal microbiota transplantation by 16s rDNA sequencing. *Neurocomputing* **2016**, *206*, 66–72. DOI:10.1016/j.neucom.2016.01.095.
15. Li, R.; Li, J.; Zhou, X. Lung microbiome: New insights into the pathogenesis of respiratory diseases. *Signal Transduct Target Ther* **2024**, *9*, 19. DOI:10.1038/s41392-023-01722-y.
16. Liwen, Z.; Yu, W.; Liang, M.; Kaihong, X.; Baojin, C. A low abundance of Bifidobacterium but not Lactobacillius in the feces of Chinese children with wheezing diseases. *Medicine* **2018**, *97*, e12745. DOI:10.1097/MD.0000000000012745.
17. Shyamala, G.; Duc, P.; Yaxun, J.; Mohammad, F.; Magddalena, H.H. ; Benjamin, U.; Adam, T.C.; David, P.; Adam, S.L.; Uma, S.S. TLR2 activation limits rhinovirus-stimulated CXCL-10 by attenuating IRAK-1-Dependent IL-33 receptor signaling in human bronchial epithelial cells. *J Immunol*; Baltimore, MD **2016**, *197*, 2409–2420.
18. Li, J.; Zhang, L.; Chen, X.; Chen, D.; Hua, X.; Bian, F.; Deng, R.; Lu, F.; Li, Z.; Pflugfelder, S.C.; et al. Pollen/TLR4 innate immunity signaling initiates IL-33/ST2/Th2 pathways in allergic inflammation. *Sci Rep* **2016**, *6*, 36150. DOI:10.1038/srep36150.
19. GMG. In response to the “Letter to editor about the article “Myelin as a regulator of development of the microbiota-gut-brain axis”” we wish to refute the concerns raised by the author. *Brain Behav Immun* **2021**, 10159–10159.
20. Thaiss, C.A.; Itav, S.; Rothschild, D.; Meijer, M.T.; Levy, M.; Moresi, C.; Dohnalová, L.; Braverman, S.; Rozin, S.; Malitsky, S.; et al. Persistent microbiome alterations modulate the rate of post-dieting weight regain. *Nature* **2016**, *540*, 544–551. DOI:10.1038/nature20796.
21. Wong, S.H.; Zhao, L.; Zhang, X.; Nakatsu, G.; Han, J.; Xu, W.; Xiao, X.; Kwong, T.N.Y.; Tsoi, H.; Wu, W.K.K.; et al. Gavage of fecal samples from patients with colorectal cancer promotes intestinal carcinogenesis in Germ-free and conventional mice. *Gastroenterology* **2017**, *153*, 1621–1633.e6. DOI:10.1053/j.gastro.2017.08.022.
22. Zhang, Y.; Wu, Q.; Zhou, M.; Luo, Z.; Lv, L.; Pei, J.; Wang, C.; Chai, B.; Sui, B.; Huang, F.; et al. Composition of the murine gut microbiome impacts humoral immunity induced by rabies vaccines. *Clin Transl Med* **2020**, *10*, e161. DOI:10.1002/ctm2.161.
23. Kim, D.I.; Song, M.K.; Lee, K. Comparison of asthma phenotypes in OVA-induced mice challenged via inhaled and intranasal routes. *BMC Pulm Med* **2019**, *19*, 241. DOI:10.1186/s12890-019-1001-9.
24. Qing, W.; Hequan, L.; Zhiyuan, Z.; Yao, Y.; Zhou, J. Prolonged ovalbumin challenge facilitates Th17 polarization in sensitized mice. *Inflam Res* **2010**, *59*, 561–569. DOI:10.1007/s00011-010-0162-z.
25. Lødrup Carlsen, K.C.; Carlsen, K.H.; Nikander, K.; Leegaard, J.; Havnen, J.; Steen-Johnsen, J.; Winsness, A. Nebulized budesonide after hospitalization for recurrent bronchial obstruction in children younger than 18 months. *Pediatr Allergy Immunol* **2001**, *12*, 159–165. DOI:10.1034/j.1399-3038.2001.012003159.x.
26. Edsbäcker, S.; Andersson, K.E.; Ryrfeldt, A. Nasal bioavailability and systemic effects of the glucocorticoid budesonide in man. *Eur J Clin Pharmacol* **1985**, *29*, 477–481.

DOI:10.1007/BF00613465.

27. Chen, T.; Zhang, B.; He, G.; Shen, C.; Wang, N.; Zong, J.; Chen, X.; Chen, L.; Li, C.; Zhou, X. Exosomes-mediated retinoic acid disruption: A link between gut microbiota depletion and impaired spermatogenesis. *Toxicology* **2024**, *508*, 153907. DOI:10.1016/j.tox.2024.153907.
28. Hao, Y.; Feng, Y.; Yan, X.; Chen, L.; Zhong, R.; Tang, X.; Shen, W.; Sun, Q.; Sun, Z.; Ren, Y.; et al. Gut microbiota-testis axis: FMT improves systemic and testicular micro-environment to increase semen quality in type 1 diabetes. *Mol Med* **2022**, *28*, 45. DOI:10.1186/s10020-022-00473-w.
29. Yang, S.; Pan, H.; Wang, T.; Zhou, X.; Fan, L.; Xiao, H.; Zhou, Z.; Xiao, Y.; Shi, D. Bacillus paralicheniformis-mediated gut microbiota promotes M2 macrophage polarization by inhibiting P38 MAPK signaling to alleviate necrotizing enterocolitis and apoptosis in mice. *Microbiol Res* **2025**, *296*, 128136. DOI:10.1016/j.micres.2025.128136.
30. Meldrum, K.; Evans, S.J.; Burgum, M.J.; Doak, S.H.; Clift, M.J.D. Determining the toxicological effects of indoor air pollution on both a healthy and an inflammatory-comprised model of the alveolar epithelial barrier in vitro. *Part Fibre Toxicol* **2024**, *21*, 25. DOI:10.1186/s12989-024-00584-8.
31. MMH; Katharina, M.; Stefan, B. Murine fecal microbiota transplantation alleviates intestinal and systemic immune responses in Campylobacter jejuni infected mice harboring a human gut microbiota. *Front Immunol* **2019**, 102272.
32. Allam-Ndoul, B.; Guénard, F.; Barbier, O.; Vohl, M.C. Effect of n-3 fatty acids on the expression of inflammatory genes in THP-1 macrophages. *Lipids Health Dis* **2016**, *15*, 69. DOI:10.1186/s12944-016-0241-4.
33. Yahao, R.; Takamichi, I.; Miao, H.; et al. Co-exposure to lipopolysaccharide and desert dust causes exacerbation of ovalbumin-induced allergic lung inflammation in mice via TLR4/MyD88-dependent and -independent pathways. Allergy, asthma, and clinical immunology: official journal of the Canadian Society of Allergy and Clinical Immunology **2019**, *15*, 82.
34. Li, Y.; Chang, L.H.; Huang, W.Q.; Bao, H.W.; Li, X.; Chen, X.H.; Wu, H.T.; Yao, Z.Z.; Huang, Z.Z.; Weinberg, S.E.; et al. IL-17A mediates pyroptosis via the ERK pathway and contributes to steroid resistance in CRSwNP. *J Allergy Clin Immunol* **2022**, *150*, 337–351. DOI:10.1016/j.jaci.2022.02.031.
35. Ravi, A.; Chowdhury, S.; Dijkhuis, A.; Bonta, P.I.; Sterk, P.J.; Lutter, R. Neutrophilic inflammation in asthma and defective epithelial translational control. *Eur Respir J* **2019**, *54*, 1900547. DOI:10.1183/13993003.00547-2019.
36. Manupati, S.; Mahaboobkhan, R.. 3. 3'- diindolylmethane hinders IL-17A/IL-17RA interaction and mitigates imiquimod-induced psoriasiform in mice. *Int Immunopharmacol* **2022**. DOI:10.9108795-108795.
37. Wanderer, A.A. Proposed pathobiologic mechanisms of hypoxia-ischemia-reperfusion in corticosteroid-resistant neutrophilic asthma and consideration of interleukin 1 targeted therapy. *Ann Allergy Asthma Immunol* **2011**, *106*, 69–72. DOI:10.1016/j.anai.2010.09.007.
38. Cooper, H.S.; Murthy, S.N.; Shah, R.S.; Sedergran, D.J. Clinicopathologic study of dextran sulfate sodium experimental murine colitis. *Lab Invest* **1993**, *69*, 238–249.

Figures

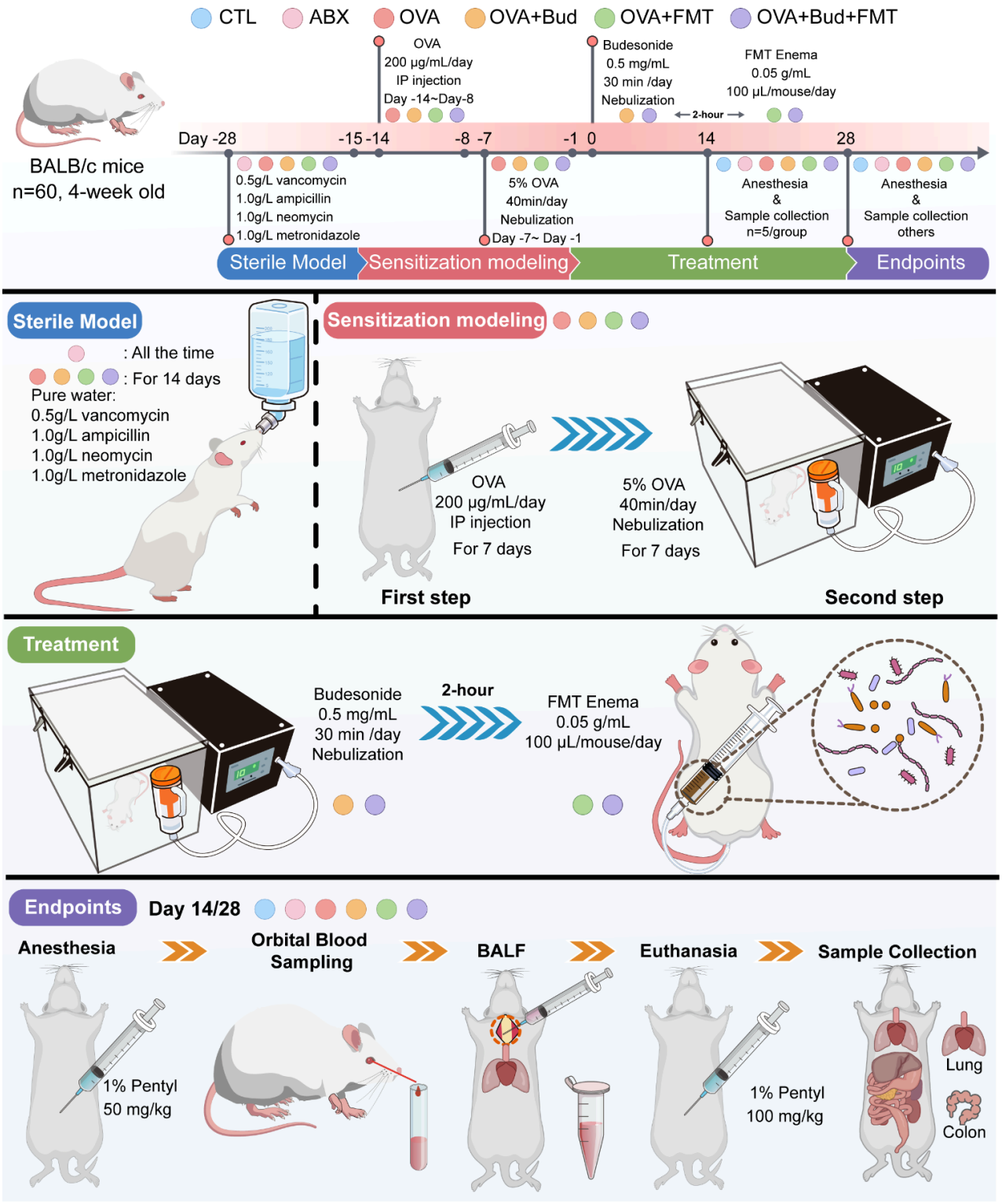


Figure 1

Flowchart of mouse model establishment procedures.

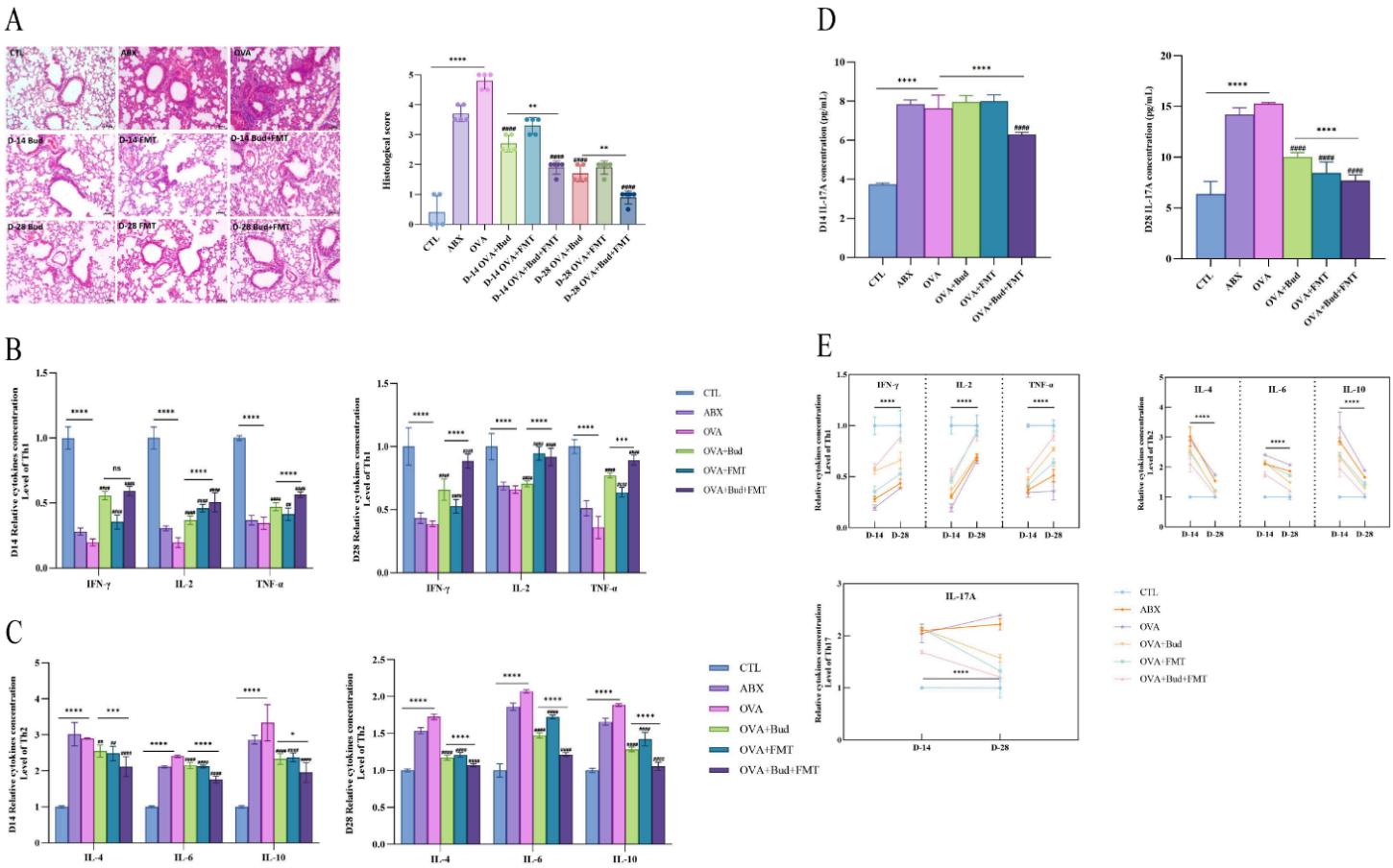


Figure 2

FMT ameliorates pulmonary inflammation and immune imbalance in allergic asthma mice. (**a**) Representative HE-stained lung sections from mice in the CTL, ABX, OVA, OVA+Bud, OVA+FMT, and OVA+Bud+FMT at D-14 and D-28. Scale bars, 50 μm. The semi-quantitative histological scores of lung inflammation. (**b**) Relative levels ofTh1-associated cytokines (IFN-γ, IL-2 and TNF-α) measured at D-14 and D-28. (**c**) Relative levels of Th2-associated cytokines (IL-4, IL-6 and IL-10) measured at D-14 and D-28. (**d**) Concentration of the Th17-associated cytokine interleukin-17A (IL-17A) measured at D-14 and D-28. (**e**) Relative concentrations of Th1-associated cytokines (IFN-γ, IL-2 and TNF-α), Th2-associated cytokines (IL-4, IL-6 and IL-10), and the Th17- associated cytokine IL-17A measured at D-14 and D-28. n=5 mice/group; $^{*}P < 0.05$, $^{**}P < 0.01$, $^{***}P < 0.001$, $^{****}P < 0.0001$, ns, not significant; $^{\#}P < 0.05$, $^{\#\#}P < 0.01$, $^{\#\#\#}P$□0.001, $^{\#\#\#\#}P < 0.0001$ versus the OVA group.

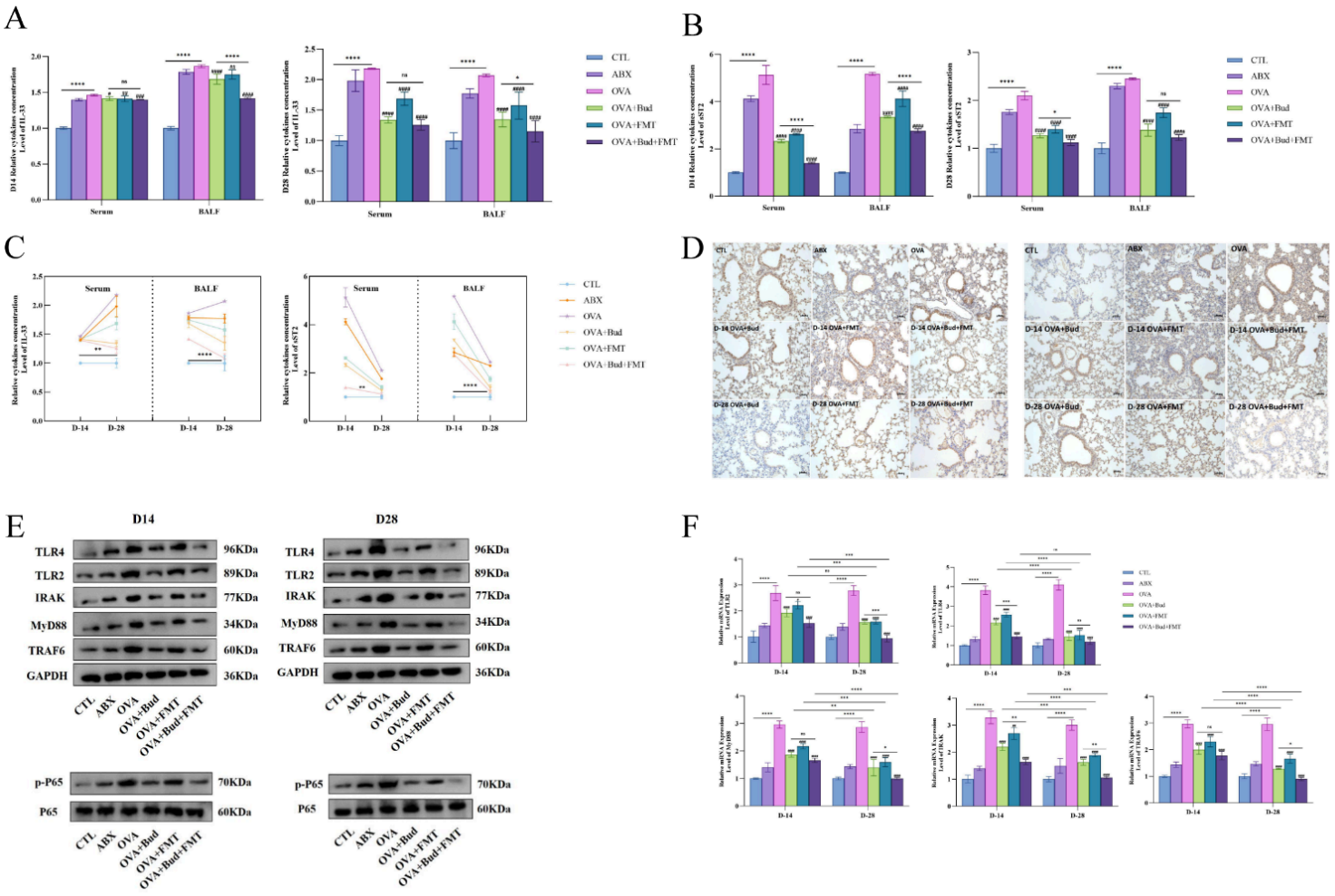


Figure 3

FMT suppresses the TLRs–IL-33/sST2 signaling axis in allergic asthma. (**a**) Relative levels of IL-33 in serum and BALF at D-14 andD-28 as determined by RT-qPCR. (**b**) Relative levels of soluble suppression of sST2 in serum and BALF at D-14 and D-28 as determined by RT-qPCR. (**c**) Relative concentrations of IL-33 and sST2 were measured at D-14 and D-28 as determined by RT-qPCR. (**d**) Representative IHC staining images of TLR2(left) and TLR4(right) in lung sections from mice in the CTL, ABX, OVA, OVA+Bud, OVA+FMT, OVA+Bud+FMT groups at D-14 and D-28. Scale bars, 50 μm. (**e**) Western blot analysis of TLR2, TLR4, IRAK, MyD88, TRAF6 and p-P65 in lung tissues at D-14 and D-28. (**f**) Relative mRNA expression levels of TLR2, TLR4, IRAK, MyD88 and TRAF6 as determined by RT-qPCR. n=5 mice/group; $^{*}P < 0.05$, $^{**}P < 0.01$, $^{***}P < 0.001$, $^{****}P < 0.0001$, ns, not significant; $^{\#}P < 0.05$, $^{\#\#}P < 0.01$, $^{\#\#\#}P$ 0.001, $^{\#\#\#\#}P < 0.0001$ versus the OVA group.

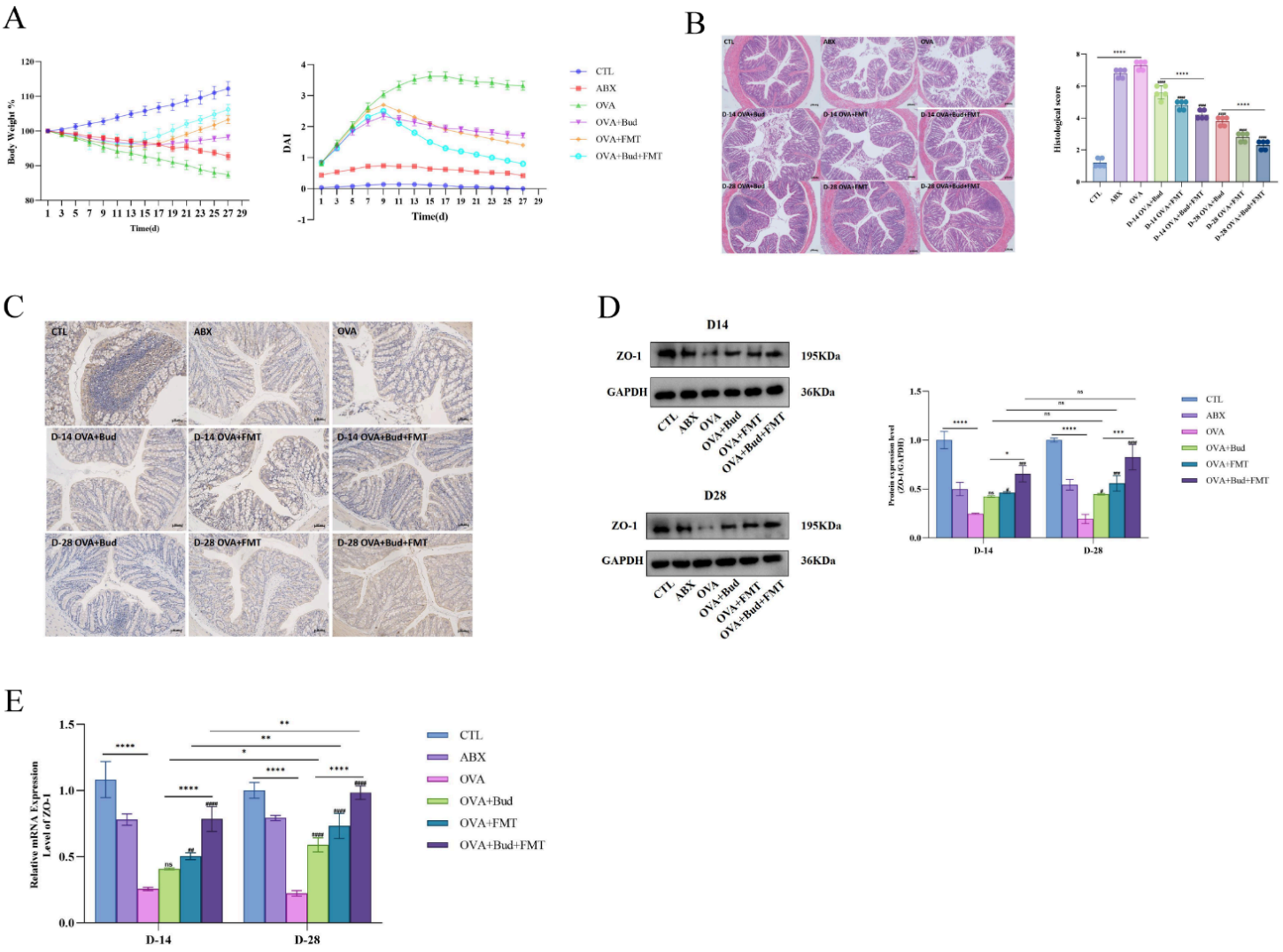


Figure 4

FMT alleviates colonic injury and promotes intestinal epithelial barrier integrity. (**a**) Changes in body weight and DAI in different groups over time. (**b**) Representative HE-stained sections of colonic tissues and corresponding histological scores at D-14 and D-28. Scale bars, 50 μm. (**c**)Representative IHC staining of ZO-1 in colonic tissues at D-14 and D-28. (**d**) Western blot analysis and quantitative densitometric analysis of ZO-1 protein expression in colonic tissues at D-14 and D-28. (**e**) Relative mRNA expression levels of ZO-1 in colonic tissues at D-14 and D-28 as determined by RT-qPCR. n=5 mice/group; $^{*}P < 0.05$, $^{**}P < 0.01$, $^{***}P < 0.001$, $^{****}P < 0.0001$, ns, not significant; $^{\#}P < 0.05$, $^{\#\#}P < 0.01$, $^{\#\#\#}P$ 0.001, $^{\#\#\#\#}P < 0.0001$ versus the OVA group.

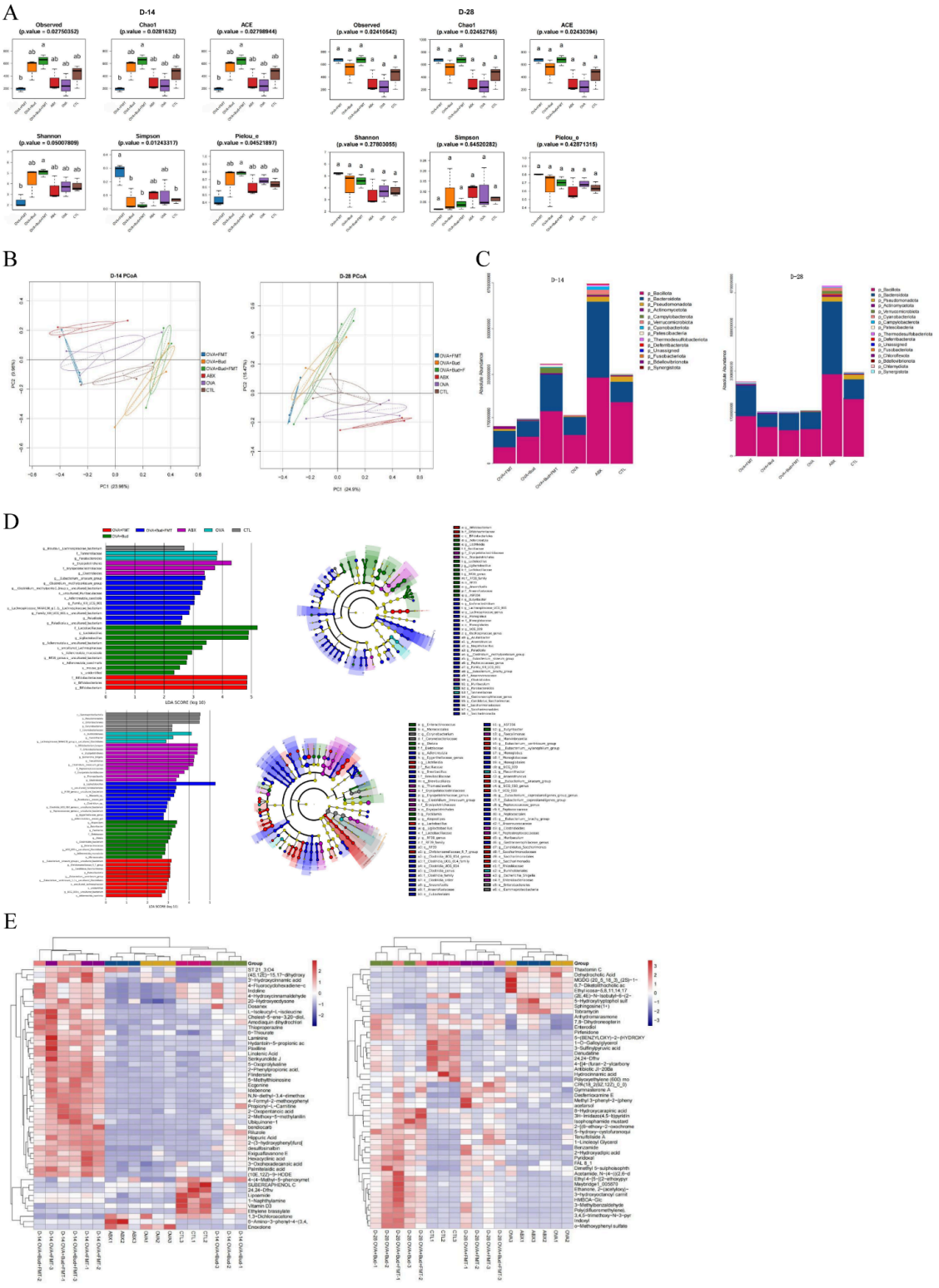


Figure 5

FMT modulates GM composition and microbiota-derived metabolic pathways. (**a**) Alpha diversity analysis of GM at D-14 and D-28. (**b**) PCoA based on beta diversity at D-14 and D-28. (**c**) Relative abundance of GM at the phylum level at D-14 and D-28. (**d**)LDA scores and LEfSe cladograms identifying differentially abundant taxa among groups at D-14 and D-28. (**e**) Heatmap of the top 50 differential metabolites across different groups at D-14 and D-28.

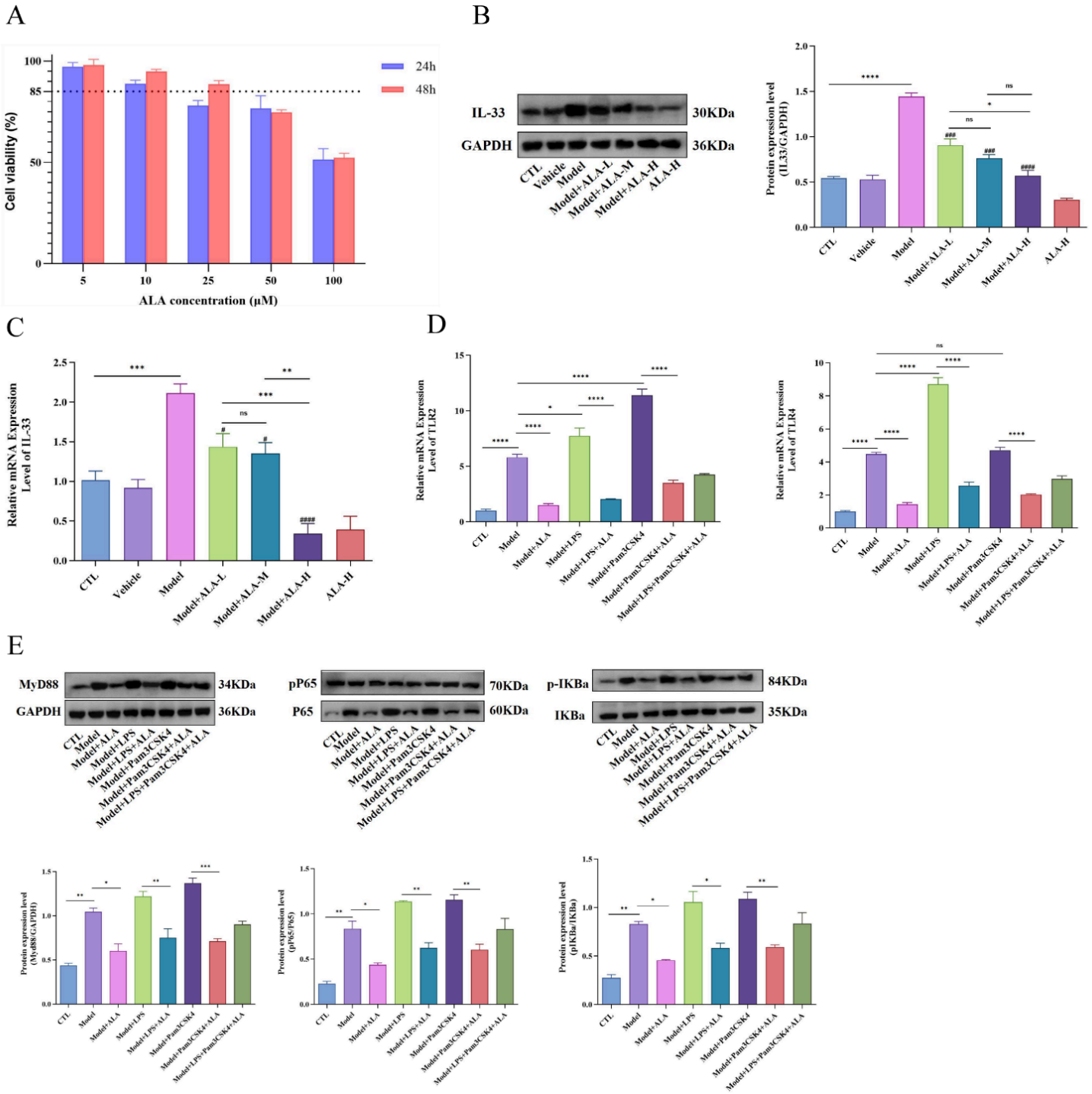


Figure 6

ALA suppresses IL-33 expression by inhibiting the TLR2/4–MyD88–NF-κB signaling pathway in MLE-12 cells. (**a**) Effects of different concentrations of ALA (0-100 μM) on the viability of MLE-12 cells after 24 h and 48 h, as assessed by CCK-8 assay. (**b**) Representative Western blot images of IL-33 protein expression in MLE-12 cells treated with vehicle, model stimulation, or increasing concentrations of ALA (low, medium and high doses) and quantitative analysis of IL-33 protein expression normalized to GAPDH. (**c**) Relative mRNA expression levels of IL-33 determined by qRT-PCR. (**d**) Relative mRNA expression levels of TLR2 and TLR4 in MLE-12 cells following model stimulation, ALA treatment and

additional stimulation with the TLR4 agonist LPS and/or the TLR2 agonist Pam3CSK4. (**e**) Representative Western blot images and quantitative analysis of MyD88, p-p65 and p-IκBα in MLE-12 cells under the indicated treatments. Each experiment was performed independently at least three times. $^{*}P < 0.05$, $^{**}P < 0.01$, $^{***}P < 0.001$, $^{****}P < 0.0001$, ns, not significant; $^{\#}P < 0.05$, $^{\#\#}P < 0.01$, $^{\#\#\#}P$ 0.001, $^{\#\#\#\#}P < 0.0001$ versus the OVA group.

Supplementary Files

This is a list of supplementary files associated with this preprint. Click to download.

- Supplementarymaterial.zip